

Regular article

Producing Ni-base superalloys single crystal by selective electron beam melting

Edouard Chauvet, Catherine Tassin, Jean-Jacques Blandin, Rémy Dendievel, Guilhem Martin *

Univ. Grenoble Alpes, CNRS, Grenoble INP, SIMaP, F-38000 Grenoble, France

ARTICLE INFO

Article history:

Received 24 December 2017

Received in revised form 22 March 2018

Accepted 26 March 2018

Available online xxxx

Keywords:

Electron beam melting

Ni-base superalloys

Single crystal

Grain selection

Crack-free

ABSTRACT

The possibility to produce Ni-base superalloy single crystals by selective electron beam melting (S-EBM) is demonstrated. The production of single crystals specimens was achieved by a tight control of the processing conditions without requiring a grain selector or a crystal seed. The melting parameters are controlled so as to promote columnar grains and intensify the competitive grain growth.

© 2018 Acta Materialia Inc. Published by Elsevier Ltd. All rights reserved.

Additive manufacturing (AM) is a breakthrough for the production of complex components providing a high degree of freedom in the design of parts and offering the possibility to tailor the microstructure. Since the pioneering work of Hunt [1,2], the magnitude and direction of the thermal gradient as well as the solidification velocity are the keys parameters to modify the solidification structure. In the literature of S-EBM (Selective Electron Beam Melting), it is suggested that changes of the melting strategies enable to alter the thermal gradient and solidification velocity to achieve different grain structures and texture. Helmer et al. [3,4] reported that grain size and morphology can be controlled. Dehoff et al. [5,6] have demonstrated that spatially controlled texture within an Inconel 718 part can be achieved. Such microstructure engineering approach was further investigated by Helmer et al. [7] and Raghavan et al. [8,9]. They showed that different scanning strategies enable to control the thermal gradient magnitude and direction resulting in different grain morphologies and sizes. Processing non-weldable Ni-based superalloys by S-EBM appears much more challenging as severe hot cracks may develop [10–12]. Ramsperger et al. have reported the possibility to produce crack-free specimens of CMSX-4 [10]. A recent investigation focused on the mechanism at the origin of the development of hot cracks in a non-weldable Ni-based superalloy fabricated by S-EBM showed that only High Angle Grain Boundaries (HAGBs) are affected by cracks while the Low Angle Grain Boundaries (LAGBs) remain systematically uncracked [12]. This suggests that if one succeeds to tailor the microstructure so as to remove any HAGB, i.e. to generate a single crystal (SX), crack-free samples can be produced. Moreover,

SXs are the most efficient way to increase the creep behaviour of Ni-based superalloys in the high temperature regime.

Achieving SX through AM is challenging. The literature dealing with the repair of SX components by AM processes is limited [13–15]. Selective Laser Epitaxy (SLE) or Direct Metal Deposition (DMD) were the first AM processes allowing the deposition of several SX layers on the CMSX-4 [14,15] or René N5 alloys [13]. If one considers the possibility to produce bulk SX using AM processing routes, the literature becomes even poorer. The possibility to generate bulk CMSX-4 single crystals by S-EBM was only reported in a conference paper by Ramsperger et al. [16].

In the present contribution, thanks to a tight control of processing parameters and strategy, crack-free bulk single crystals of a non-weldable Ni-based superalloy are produced by S-EBM without requiring a crystal selector or a seed.

The studied alloy is a non weldable Ni-Co-Cr-Mo-Al-Ti-B Ni-based superalloy containing significant amounts of Cr, Co and Mo with Ti + Al wt% = 8.6. The exact chemical composition cannot be indicated for industrial confidentiality reasons. The prealloyed powder was produced by gas-atomization and provided by ERASTEEL. The as-received powder particles exhibit mostly a spherical morphology with some satellites ($D_{50} = 77 \mu\text{m}$ and powder bed relative density = 53.6%, see [12] for more details).

The prealloyed powders were used into an ARCAM A1 EBM machine operating at 60 kV accelerating voltage under a controlled pressure of 2.10^{-3} mbar. The powder was deposited by 50 μm thick layers on a stainless steel plate, then slightly sintered with a defocused beam and finally selectively melted according to the input CAD geometry. The operating temperature was ~ 1020 °C. Samples with dimensions of $23 \times 23 \times 30$ mm melted in manual mode,

* Corresponding author.

E-mail address: guilhem.martin@simap.grenoble-inp.fr (G. Martin).

i.e. with the automatic ARCAM functions disabled, were fabricated by varying the scan speed ($v = 500\text{--}1500$ mm/s) and beam power ($P = 225\text{--}600$ W). Such a processing window was chosen to ensure a high bulk density ($>99.5\%$, no lack-of-fusion defects) while avoiding significant overmelting leading to uneven surfaces [3,17]. This was achieved by using linear energies ($E_l = P/v$) between 0.3 and 0.6 J/mm. The melting strategy and focus offset (20 mA) were held invariants. The melting strategy consists of scanning the area defined by the CAD file in a snake-line way with a line offset of 0.1 mm and a line order set to 1. The scanning direction was rotated by 90° after every layer. The building time for one layer was about 160 s for a build consisting of 9 samples.

The microstructures were characterized by optical microscopy, SEM (ZEISS Gemini SEM500) and EBSD along the longitudinal cross sections (XZ plane). The microstructures were revealed using a fresh Glyceregia etchant [12]. EBSD measurements were performed using the OIM-TSL software.

A typical as-built sample is shown in Fig. 1a. The observations were done in the XZ plane, see Fig. 1a. Fig. 1b shows an example of the region located just below the top surface. Fig. 1b is analogous to the typical microstructure of a weld since the melted zone, the heat affected zone and the “base material” (built material unaffected thermally by the melted zone) can be distinguished. The terminology “base material” might be excessive here as it can be thermally affected but only during the preheating stages. The height of the last melted zone (depth of the melt pool) can be estimated based on the microstructural characterization performed in the top region, see example in Fig. 1b. High power combined with slow scanning speed, corresponding to the highest linear energy ($E_l = 0.6$ J/mm), lead to the deepest melt pools. As expected, for a given power, the melt pool depth increases when the scanning speed decreases. Similarly, for a given scanning speed, the melt pool depth increases with power. Within the processing window selected for a 50 μm layer thickness, melting occurs from 3 up to 12 layers down corresponding to melt pool depths varying between 150 μm ($E_l = 0.3$ J/mm) and 600 μm ($E_l = 0.6$ J/mm).

The region just below the top surface is of particular interest because it is the only region where the dendritic microstructure inherited from the solidification can be observed. Below this region, the dendritic microstructure is partly or even completely erased by the fact that the underlying layers have been significantly thermally affected during the addition of new layers. It was thought that this rather complex thermal path undergone by the underneath layers could be seen as a sort of solutionizing heat treatment erasing the dendritic microstructure and changing drastically the precipitation state as shown in [12]. Primary dendrite trunks can be easily seen in this last melted zone as shown in Fig. 1c. Primary dendrite arm spacing (PDAS), estimated by the

intercept method, was found to vary between ~ 10 and 30 μm depending on the linear energy. The highest linear energy ($E_l = 0.6$ J/mm) within the identified processing window gives the highest PDAS (about 30 μm). Such PDAS values can be used to infer information regarding the cooling rate from literature data correlating PDAS with cooling rate for several Ni-based superalloys [18]. A PDAS of 10 μm suggests a cooling rate of the order of ~ 500 $^\circ\text{C/s}$ while a PDAS of 30 μm corresponds to a cooling rate of ~ 30 $^\circ\text{C/s}$ (one order of magnitude smaller) [18]. PDAS values with the same order of magnitude though a bit smaller (between 3 and 10 μm) were reported recently for Inconel 718 [9]. This is consistent with the localized melt-scan strategy used in [9] leading to higher cooling rates whereas a raster melt-scan strategy was used here.

Microstructural observations in the entire XZ cross section reveal typical features of parts manufactured by AM. The edges of the samples were more or less affected by the local thermal conditions since in those regions, heat was not only extracted by the built material but also by the surrounding powder bed. In this contribution, the attention is focused on the central region of the samples. Melting parameters leading to deep melt pools were deliberately selected to promote epitaxial growth along the building direction. Columnar grains growing epitaxially along the build direction across several layers were found in the central region, see Fig. 2a–c. Those columnar microstructures are typical of directionally solidified materials, see e.g. [19,20].

Over the first millimeters, all samples exhibit a similar microstructure consisting of relatively narrow columnar grains (region A in Fig. 2a–c). With further addition of layers, texture develops and becomes strongly oriented with a [001]-fiber texture and larger columnar grains grow [12]. The main microstructural differences between the samples are (i) the columnar grain width and (ii) the selection of grain orientation which is more or less pronounced depending on the processing parameters. Fig. 2a shows a sample exhibiting a homogeneous microstructure with relatively fine columnar grains (grain width ~ 100 μm). This sample was melted using a linear energy of 0.3 J/mm. The associated melt pool depth was found to be 150 ± 10 μm and the PDAS, estimated to 13 ± 1 μm . In Fig. 2b is shown a sample exhibiting a gradient of columnar grain width, their width being close to 1 mm in the upper part (Fig. 2b). The melt pool depth was about 260 ± 10 μm and the PDAS about 16 ± 1 μm . Fig. 2c, melted with a linear energy of 0.45 J/mm, shows another example where the gradient of columnar grain width was strengthened (columnar grain width of several millimeters in the upper part) using parameters leading to a melt pool depth of 366 ± 10 μm and a PDAS of 23 ± 1 μm . Those observations suggest that with appropriate changes of the processing parameters, the gradient of columnar grain width can be exacerbated by intensifying the grain growth competition until obtaining a single grain orientation after <10 mm of built material. This was achieved

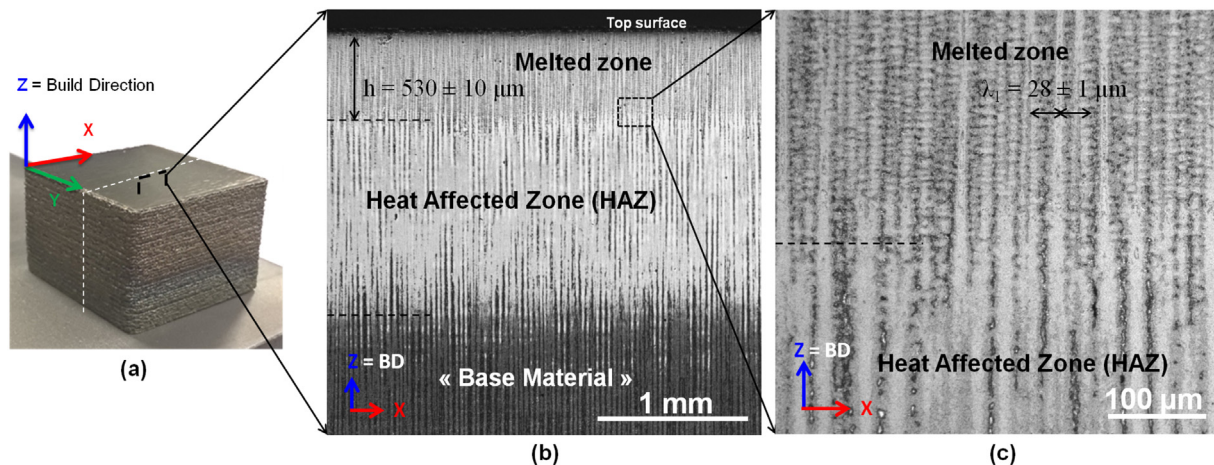


Fig. 1. (a) Typical S-EBM as-built sample. Optical micrographs showing (b) an example of the region located just below the top surface and (c) the dendritic microstructure of the last melted layer.

Download English Version:

<https://daneshyari.com/en/article/7910437>

Download Persian Version:

<https://daneshyari.com/article/7910437>

[Daneshyari.com](https://daneshyari.com)